3

Electromagnet force control

3.1 Introduction

The multivariable vehicle suspension control system proposed in Chapter 1 requires electromagnetic force actuators which are independent, and suitably linear and stable, in order to decouple and control the vehicle mode motions successfully. This chapter describes the steps involved in the synthesis and validation of a novel electromagnet force control scheme which meets the above requirements.

The open-loop force/voltage transfer function of the electromagnet is first examined to identify the dynamic structure and the parameters which characterise the experimental suspension electromagnet. Existing force control strategies, which use linear algorithms, are then examined and found to be unsatisfactory for providing independent and linear force actuation. A novel control scheme, employing a detailed nonlinear model of the electromagnet, is proposed to meet the force actuation requirements. After describing the design of the proposed force controller, the results of some experimental performance tests are presented and discussed. Finally, some conclusions are drawn on the work described in this chapter.

Before examining the electromagnet transfer function, the operational envelope for the experimental suspension electromagnet is defined, and some operational parameters are identified and discussed.

3.2 Operational envelope

The experimental electromagnet has a mass of 7.3 kg and was designed to support a maximum load of about 50 kg, giving a lift/weight ratio of about 7. A 50 kg load calls

for a maximum lift force capability of about 550 N to allow for some acceleration of the suspended load. The design of the experimental electromagnet results in a large leakage flux which limits the maximum air gap to about 5 mm for a lift force of 550 N (see Figure 2.7). This allows a nominal operating air gap of 3 mm, with a deflection of ±2 mm, to be realised. Mechanical limit stops are positioned to restrict the air gap range to 0.5-5.5 mm. The current range required to suspend 50 kg is 3.5-20 A for air gaps of 1-5.5 mm respectively. This gives a power/lift ratio of about 1.6 W/kg at the nominal operating air gap.

The minimum suspended mass for the experimental suspensions is 15 kg per electromagnet. Using Equation 2.22, the predicted air gap flux density varies from about 0.35-0.65 Tesla over the full operational envelope. The corresponding predicted electromagnet core flux density using Equation 2.24 is 0.45-1.50 Tesla. The operational envelope for the electromagnet force actuator is summarised in Table 3.1. The power/lift and lift/weight ratios for the experimental electromagnet are very similar to those achieved by electromagnets with a nominal suspension load of 250-1000 kg.[49]

Table 3.1 Operational envelope for the electromagnet

Parameter	Operating range
Lift force	0-550 N
Suspended mass	15-50 kg
Air gap	3 mm ±2 mm
Current	0-20 A

3.3 Electromagnet transfer function

A transfer function for the electromagnet is now derived to characterise its dynamic behaviour and to analyse the nature of the force instability. The approximate model of the electromagnet developed in Section 2.3.1 is used as the starting point. This model is linearised around a nominal operating point to permit modelling of the electromagnet in the frequency domain using the Laplace operator[50] s.

Since the electromagnet is in practice excited by a variable voltage source, the electromagnet force/voltage transfer function is derived and the location of the open-loop poles and zeros is identified. Figure 3.1 illustrates the configuration of the electromagnet and track and the variable nomenclature used in this chapter. To simplify the analysis, the natural frequency of the electromagnet reaction rail is assumed to be sufficiently high to be neglected.

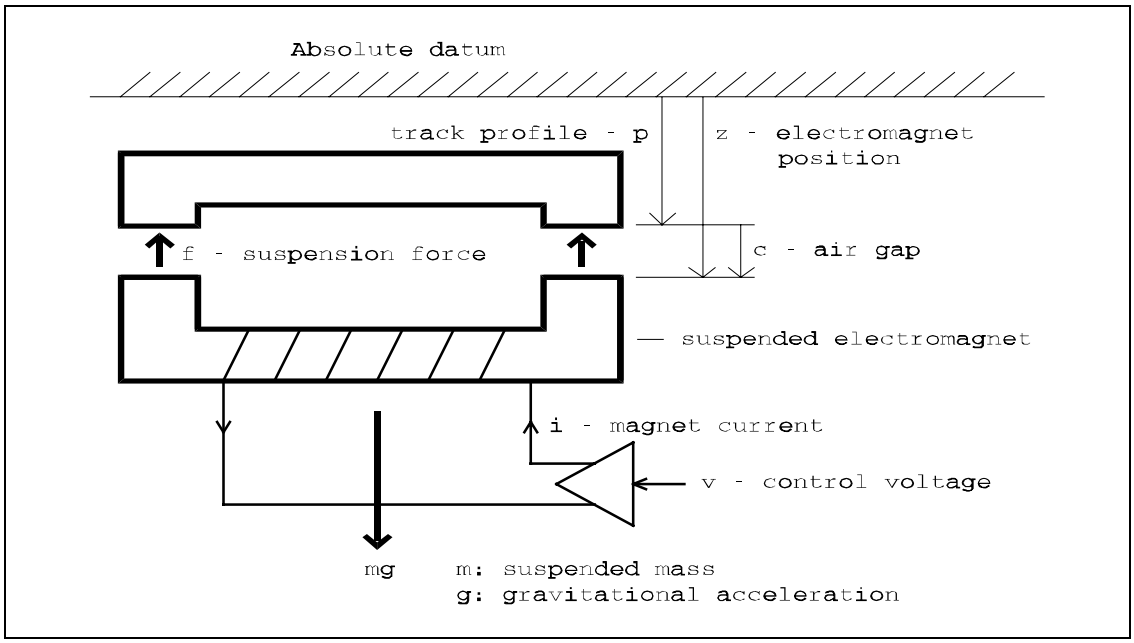

Figure 3.1 Electromagnet and track configuration

Four equations which characterise the electromagnet motion for small perturbations around a nominal operating point (i_o, c_o) are identified. These are then combined to form the force/voltage transfer function. All equations are expressed in the frequency domain using the Laplace operator s.

The air gap flux is the key element in the operation of the electromagnet, and it is approximately proportional to the coil current divided by the air gap (see Equation 2.27). This is linearised for small perturbations by:

$$\Delta\Phi(s) = k_{\phi i}\,\Delta I(s) - k_{\phi c}\,\Delta C(s) \qquad \textit{where} \quad k_{\phi i} = \frac{\partial\phi(i_o,c_o)}{\partial i}, \quad k_{\phi c} = -\frac{\partial\phi(i_o,c_o)}{\partial c} \qquad \textbf{3.1}$$

and where ΔC, $\Delta\Phi$, and ΔI are the perturbations of air gap, its flux, and current respectively, and the partial derivative coefficients, $k_{\phi i}$ and $k_{\phi c}$ are both positive.

The electromagnet force, which is approximately proportional to the square power of the air gap flux (see Equation 2.25), is linearised by:

$$\Delta F(s) = k_{f\phi}\Delta\Phi(s) \qquad where \quad k_{f\phi} = \frac{\partial f(i_o,c_o)}{\partial \phi} \tag{3.2}$$

and where ΔF is the force perturbation, and the partial derivative coefficient $k_{f\phi}$ is positive.

The acceleration of the suspended load due to the electromagnet force is now given by:

$$s^2\Delta C(s) = -\frac{\Delta F(s)}{m} \tag{3.3}$$

where m is the suspended mass.

The final equation determines the relationship between electromagnet coil voltage, air gap flux, and coil current (see Equation 2.26). This relationship is expressed by:

$$\Delta V(s) = sN\Delta\Phi(s) + R_{coils}\Delta I(s) \tag{3.4}$$

where ΔV is the coil voltage perturbation, N is the number of coil turns, and R_{coils} is the coil resistance.

The force/voltage transfer function for the electromagnet is now obtained by substituting current from Equation 3.1, flux from Equation 3.2, and force from Equation 3.3, into Equation 3.4. The substitutions are detailed in Appendix B and result in:

$$\frac{\Delta F(s)}{\Delta V(s)} = \frac{k_{f\phi}k_{\phi i}}{R_{coils}} \frac{s^2}{\left(s^3 Nk_{\phi i}/R_{coils} + s^2 - k_{f\phi}k_{\phi c}/m\right)} \tag{3.5}$$

This is more conveniently expressed as:

$$\frac{\Delta F(s)}{\Delta V(s)} = \frac{k_i}{R_{coils}} \frac{s^2}{\left(s^3 T_{flux} + s^2 - k_c/m\right)} \tag{3.6}$$

where:

$$k_i = k_{f\phi} k_{\phi i} = \frac{\partial f}{\partial \phi} \cdot \frac{\partial \phi}{\partial i} = \frac{\partial f}{\partial i}, \qquad k_c = k_{f\phi} k_{\phi c} = \frac{\partial f}{\partial \phi} \cdot \frac{\partial \phi}{\partial c} = \frac{\partial f}{\partial c}, \tag{3.7}$$

$$T_{flux} = T_{eddy} + T_{coil}, \qquad T_{coil} = N k_{\phi i} / R_{coils}$$

The partial derivative coefficient k_i represents the force/current gain factor, whilst k_c represents the magnitude of the electromagnet's negative stiffness. T_{flux} is the total flux lag time constant (see Section 2.4.6), which is comprised of T_{eddy}, the eddy current time constant, and T_{coil}, the coil time constant (see Appendix B).

Equation 3.6 shows that the force/voltage transfer function has two zeros at the origin of the *s*-plane and three poles. The negative electromagnet stiffness generates a positive denominator root, which places one of the poles in the right-hand side of the *s*-plane,[51] thus producing an open-loop unstable force. Figure 3.2 illustrates the open-loop electromagnet force/voltage transfer function, with the scope of the nonlinear elements denoted by the two dashed boxes. The configuration of the eddy current flux lag loops is identical to that of the coil current flux lag loop, but with a larger resistance to reflect the smaller eddy current time constant. The eddy current loops are omitted from Figure 3.2 for the sake of clarity. The open-loop transfer function is augmented in Figure 3.2 with a second-order model of a flexible track which shows how the track motion couples with that of the electromagnet. The track model has a natural undamped frequency, ω, and damping ratio, ζ.

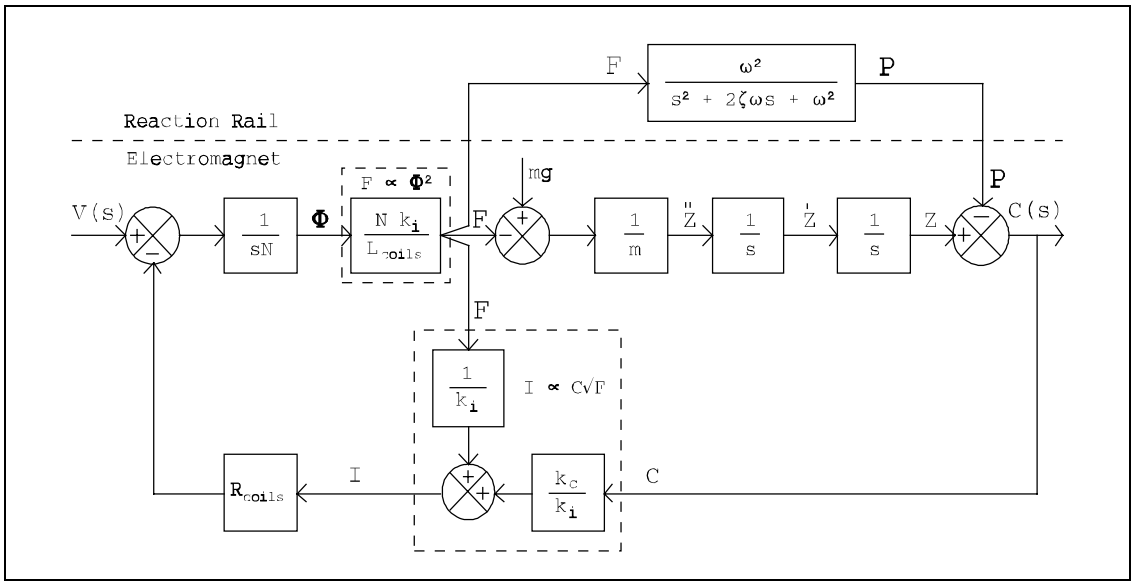

Figure 3.2 Block diagram of the electromagnet system

Table 3.2 shows how the measured parameters of the experimental electromagnet vary as a function of air gap and suspension force. The partial derivative coefficients defined in Equation 3.7, namely k_i and k_c, are calculated from the measured data used to produce the graph shown in Figure 2.7. The coil and eddy current time constants are taken from the measured data summarised in Tables 2.6 and 2.7 respectively.

Table 3.2 Linearised electromagnet model parameters

Air gap / **Parameter**	**1 mm**	**3 mm**	**5 mm**	**Max /min**
k_i	140-400 N/A	50-90 N/A	25-50 N/A	16
k_c	260-950 N/mm	95-350 N/mm	60-150 N/mm	16
T_{coil}	111 ms	85 ms	72 ms	1.5
T_{eddy}	4.6 ms	3.0 ms	2.1 ms	2.2
Notes: The coefficients k_i and k_c were measured over the force range of 150-550 N				

Due to the nonlinear nature of the electromagnet, the location of the poles of the transfer function varies with the operating point. The unstable pole reaches a maximum value of s = 77, when k_c=950 N/mm, m=15 kg, and T_{flux}=0.1 s, whilst the two remaining poles form a complex conjugate pair at s = -44 ±70j. The worst case instability time constant is therefore 13 ms.

In order to be able to neglect the effects of track flexibility and hence vibration, the track poles must be sufficiently separated from the electromagnet force poles. For the open-loop voltage controlled electromagnet, the track poles should ideally have frequencies of at least 16 Hz. The acceptable natural frequency for any closed-loop electromagnet configuration requires adequate separation of the track poles from the dominant poles of closed-loop response.

3.4 Force control strategies

The force/voltage transfer function of the electromagnet has been shown to be open-loop unstable due to the electromagnet's negative stiffness. A control strategy is now needed to provide electromagnetic force actuation with sufficient stability, accuracy, linearity, and bandwidth.

The force actuation stability is most conveniently expressed in terms of the residual electromagnet stiffness that is superimposed upon the controlled electromagnet force. The acceptable level for residual stiffness clearly depends on the requirements of the system using the electromagnet force actuator. For this application, the suspension control system uses a suspension stiffness gain of 250 N/mm and is designed to accommodate total transducer errors of up to ±25% (see Section 4.4.2). Therefore, a force accuracy of ±20% with a corresponding residual stiffness of up to ±50 N/mm will not significantly impair the suspension controller response. The linearity of the force actuators will affect the success of the vehicle mode decoupling (see Chapter 5) and so a force nonlinearity of no more than 10% is acceptable.

The suspension controller requires a force actuation bandwidth of about 50 Hz or more (see Section 4.4.3). The ideal force actuation transfer function therefore consists of a single pole low-pass filter with a time constant ≤ 3.2 ms. For small force perturbations, a linear approximation between flux and force can be assumed. The dynamic behaviour of the electromagnet force and flux is therefore considered to be equivalent for the purpose of developing a force control strategy.

The most direct method to reduce the electromagnet force instability, to improve its linearity, and to increase its force actuation bandwidth, is to apply force feedback, or some functionally equivalent feedback such as acceleration or air gap flux. An alternative approach is to target the cause of the instability, and use air gap feedback to reduce the instability. Since the largest flux time constant for the force/voltage transfer function is about 100 ms, an air gap feedback strategy must be augmented by an additional technique to increase the force actuation bandwidth. Before discussing these force control strategies, it is useful to consider the constraints imposed by the electromagnet power control hardware.

In order to achieve an acceptable weight and cost for the electromagnet power control hardware, the power conversion efficiency must be high, and the use of a switch-mode power controller rather than a linear one is therefore required.[52] This imposes an

upper limit on the voltage actuation bandwidth which is determined by the required voltage and current ratings, and the type of semiconductor device used to switch the power.[53] An additional constraint on the power controller performance is due to the provision of a finite voltage source, with the attendant potential problems of voltage and hence current slew-rate saturation.

The steady-state electromagnet current ripple which arises due to the use of a switch-mode power controller,[54] causes the magneto-motive force of the electromagnet to experience a similar superimposed oscillation. This continuous cycling of the magneto-motive force increases the effective differential permeability of the core material for small current perturbations. The use of a switch-mode controller therefore ameliorates the control problems caused by the magnetic hysteresis of the electromagnet and track cores.

3.4.1 Force feedback

The open-loop force/voltage transfer function (see Equation 3.6) has two zeros at the origin and three poles, one of which is located in the right-hand side of the s-plane, thus making the open-loop system unstable. However, the two zeros at the origin suggest that if sufficient force feedback is applied, the unstable pole can be drawn in close to the origin, thus reducing the force instability. Figure 3.3 illustrates the closed-loop root locus of the electromagnet for a force feedback gain varying from 0 to 120. The maximum gain is determined by limiting the time constant of the fast 'flux lag' pole to 1 ms to accommodate an acceptable minimum response time for the power controller. Attempts to use excessive gain would result in the additional pole due to the power controller causing the left branch of the root locus to split away from the real axis. The resultant pair of high frequency complex conjugate poles would produce an undesirable oscillatory force response.

Figure 3.3 shows that the use of force feedback can improve the worst case time constant of the unstable pole from its open-loop value of 13 ms to 44 ms. Since the closed-loop stiffness is inversely proportional to the square power of the unstable pole time constant,[55] the effective negative stiffness is reduced by a factor of 11.

The principle problem with applying force feedback is that of measuring the force. In the case of a single electromagnet suspending a load many times its own weight, a force transducer could be located between the electromagnet and its load. However, for the

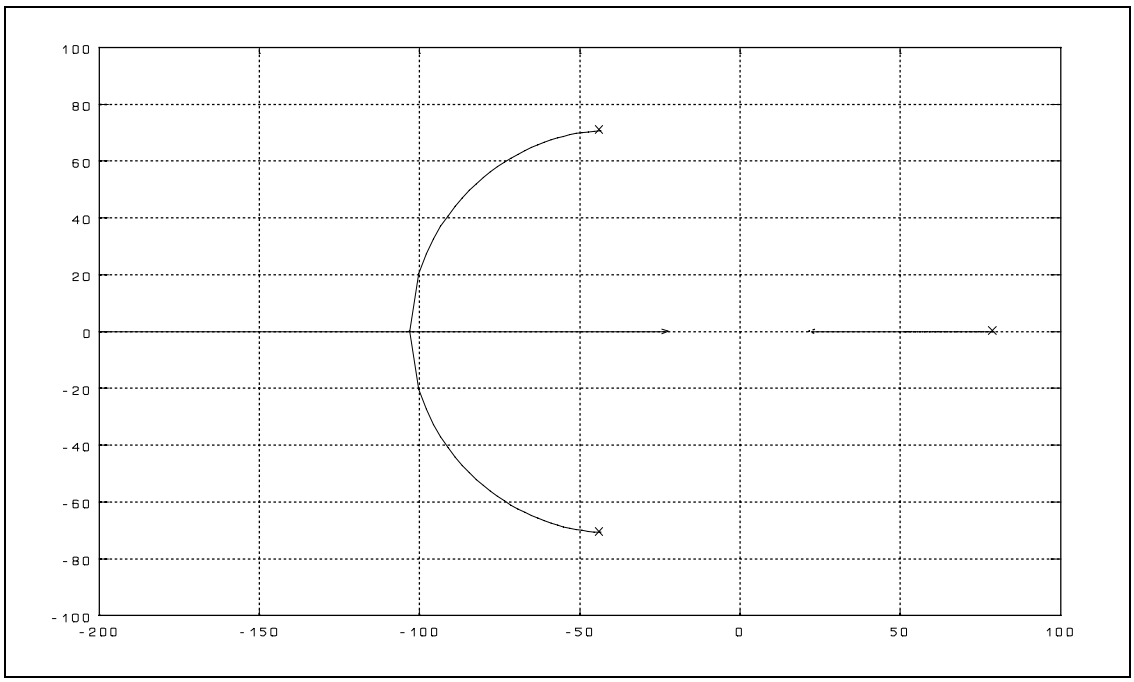

Figure 3.3 Closed-loop root locus for force feedback
(k_c = 950 N/mm, m = 15 kg, T_{flux} = 116 ms, Gain=0-120)

experimental vehicle, the measured force would suffer disturbances from the other electromagnets which are directly coupled to the vehicle chassis. Since independent electromagnet stabilisation is required, it is unacceptable to transform the electromagnet instability into a multi-variable instability problem. Therefore, direct force measurement and feedback is not a feasible option. Flux and acceleration are two possible substitutes for force feedback, so these are considered next.

3.4.2 Flux feedback

Since the electromagnet lift force is proportional to the square power of the air gap flux (see Equation 2.25), the r.m.s. level of the flux over the entire pole face area represents the lift force. This factor complicates matters because the pole face flux distribution is not always uniform. This is due to three dominant factors. Firstly, when changes in flux are demanded, eddy currents in the electromagnet and track cores cause flux to be concentrated near the pole edges during the flux transient. Secondly, the motion of an electromagnet along its track produces a similar effect, with track-borne eddy currents causing a flux lag which is distributed spatially along the length of the electromagnet pole face and across its width. Finally, gaps between track joints can cause local flux disturbances.

Two different transducers have been used to measure flux in electromagnetic suspension systems, namely Hall plate devices and search coils. Hall plate sensors[56] must be mounted near the electromagnet pole face to minimise the measurement of leakage flux. This exposed location is environmentally harsh and the electromagnet core experiences both low and very high temperatures which can cause problems with the delicate Hall plate devices. Positioning the sensor on the pole face is an additional problem due to the non-uniform distribution of flux across the pole face area. Use of laminated electromagnet and track cores can significantly reduce the flux distribution problem, but it is an expensive option. Alternatively, a number of sensors can be used, distributed over the pole face to provide sufficient measurement accuracy and also redundancy to cope with device failures.

Hall plate sensors can enable excellent flux control, both dynamically and in the steady-state, although a nonlinear controller is needed for linear force actuation. However, due to their questionable robustness, they have not advanced from laboratory prototypes.

The prime benefit of flux control can be achieved more readily and robustly through the use of a search coil wound around the electromagnet poles, close to the pole faces. The coil voltage gives a measure of the rate of change of flux which must be integrated to provide a measure of the flux. To avoid problems due to integrator drift, a low frequency roll-off is required. The resultant lack of a d.c. response does not impair the stabilisation function since the flux dynamics are the problem, not the steady-state flux. However, linear control of the lift force is impossible since there is no absolute flux level measurement.

The merits of the search coil sensor are that it senses the average flux level over the whole pole face area, and it provides a cheap and robust method of reducing the force instability. However its major disadvantage for this application is that it cannot produce a linear force actuator.

3.4.3 Acceleration feedback

The final alternative to direct force measurement is to measure electromagnet acceleration to derive the lift force. An acceleration signal is required by the suspension controller, and is obtained by attaching an accelerometer to the electromagnet. If a conventional secondary suspension is used, this technique is

available directly. However, the rigid coupling of the electromagnets and accelerometers to the chassis of the experimental vehicle leads to a tightly coupled multi-variable instability problem. Acceleration feedback, like force feedback, is thus incapable of providing independent electromagnet stabilisation.

3.4.4 Air gap and current feedback

The electromagnet is open-loop unstable due to its negative stiffness coefficient. The instability of the electromagnet force can therefore be reduced by using air gap feedback with the controller stiffness set as close as possible to the magnitude of the open-loop electromagnet stiffness. The force actuation time constant can then be significantly reduced by using high gain current feedback. A current loop gain of 100 is sufficient to reduce the coil current lag time constant from a worst case value of 110 ms down to approximately 1 ms. The transfer function of the open-loop current controlled electromagnet is given by Equation 3.6, but with T_{flux} now given by:

$$T_{flux} = T_{eddy} + \frac{T_{coil}}{k_{amp}} \qquad \textbf{3.8}$$

where k_{amp} is the loop gain of the current controller (see Appendix B). The worst case time constant of the unstable pole for the current controlled electromagnet is 5.6 ms (for k_{amp} = 100). The higher force actuation bandwidth incurs the penalty of a faster instability time constant relative to a voltage controlled electromagnet.

Air gap and current feedback can theoretically provide a stable and linear force actuator, but only for a single operating point in terms of air gap and force. The problem with this technique is that the negative stiffness coefficient (see Table 3.2) varies by a factor of about 16 over the full operational envelope of the electromagnet. The closed-loop root locus for the current controlled electromagnet with air gap feedback (see Figure 3.4) shows that the closed-loop force becomes more unstable as the air gap feedback gain error increases. If the feedback gain is too high, a pair of unstable complex conjugate poles replaces the single unstable pole which is present if the gain is too low. If the feedback gain is approximately equal to the electromagnet stiffness, the two poles near the origin can be considered to cancel with the two zeros at the origin. The resultant force transfer function is then dominated by the flux lag pole.

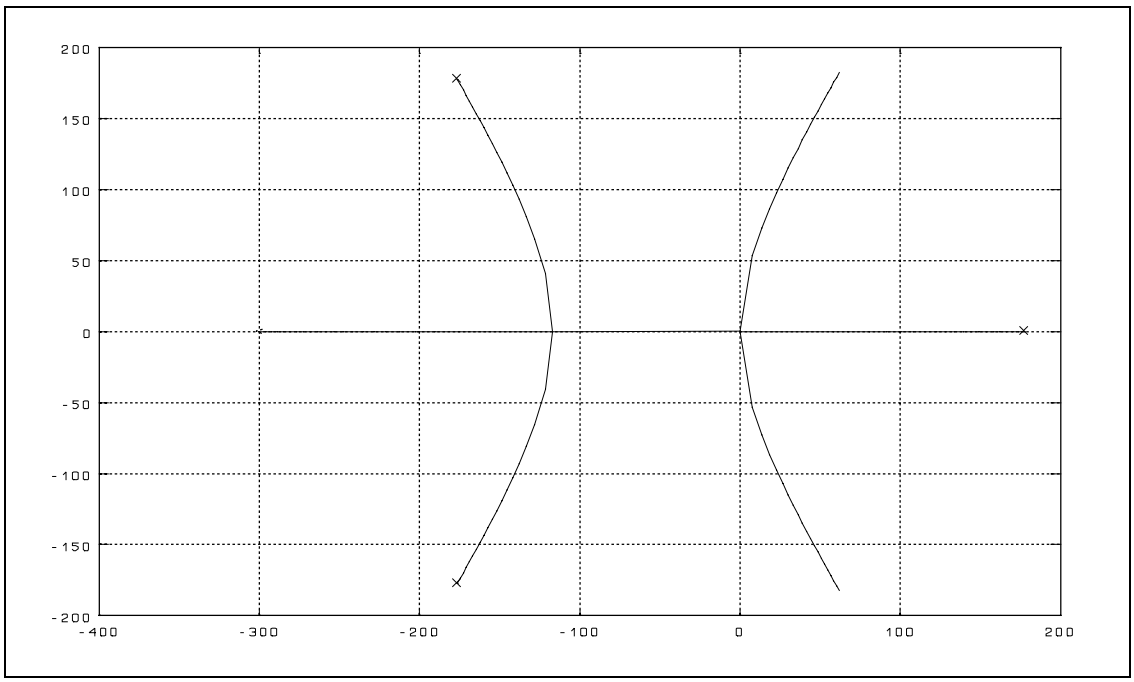

Figure 3.4 Closed-loop root locus for air gap and current feedback (k_c=950 N/mm, m=15 kg, T_{flux}=5.7ms, Gain=0-2k_c)

In order to match the variation in the open-loop stiffness over the full operational envelope, a nonlinear control algorithm is required. A disadvantage of this technique is that in order to achieve accurate gain scheduling, the required control algorithm must embody a complex model of the electromagnet (see Chapter 2). If sufficient accuracy can be achieved in the model and signal measurements, a reasonably stable and linear force actuator is theoretically possible. A further disadvantage associated with air gap feedback stabilisation, is that unlike force or flux feedback, air gap feedback does not encompass the magnetic hysteresis of the electromagnet and track cores.

Accurate measurement of the r.m.s. air gap over the full length of the electromagnet is ideally required. In practice, a large area sensor and/or a number of smaller sensors could be used to measure the average air gap. For example, using triple mode redundancy, three sensors could provide average air gap measurement, with a graceful degradation of accuracy if one of the sensors failed. Various industrial sensors using inductive, capacitive and eddy-current techniques[57] are available for non-contacting displacement measurement.

3.4.5 Proposed force control strategy

The major problem associated with producing a well controlled suspension force from an electromagnet stems from the variation of the parameters of the open-loop transfer function rather than the fact that it is unstable. However, in reality it is only the parameters of the linearised model which vary. The parameters of the nonlinear models developed in Chapter 2 are mostly constant. The coefficient parameters of the static force characteristic are determined by the physical dimensions of the electromagnet and track, and the permeability of air, both of which are essentially constant. The dynamic behaviour of the electromagnet is only slightly less ideal since temperature affects the coil resistance and core resistivity which in turn affects the coil current and eddy-current time constants respectively. With such detailed models of the nonlinear behaviour of the electromagnet available, it would be unwise to discard most of the information in order to use only classical linear control algorithms.

The only force feedback scheme which is suitably robust is flux derivative feedback using a search coil. This can stabilise the electromagnet force but it cannot provide linear force actuation. For electromagnetically suspended vehicles which use conventional secondary suspensions, the electromagnets are effectively decoupled by the secondary suspensions and they can therefore be considered to be independent. For such systems, flux derivative feedback and/or acceleration feedback is employed[58,59] to stabilise and linearise the force actuation.

Alternatively, since air gap feedback is required by the suspension controller, air gap feedback stabilisation can be used with no additional transducer requirements. However, to achieve satisfactory force stability and linearity, the air gap feedback gain must be changed dynamically as a function of the operating point. The proposed central element of the electromagnet force controller is therefore, air gap feedback into a nonlinear model of the electromagnet static force characteristic.

The force controller must increase the open-loop force actuation bandwidth to the 50 Hz required by the suspension controller. This corresponds to a force actuation time constant of about 3.2 ms. The force time constant for the electromagnet is approximated by the flux time constant which is composed of the coil and eddy current lag time constants (see Equation 3.7). Since the worst-case open-loop coil and eddy current time constants (see Table 3.2) are 111 ms and 4.6 ms respectively, both of these time constants must be reduced. The massive reduction required for the coil time constant can be most robustly achieved through the use of high gain current feedback,

so that is the proposed method. The current controller also enables coil resistance changes due to varying temperature to be neglected. The additional hardware complexity of an electromagnet current controller over a voltage controller is not great and it can readily provide safe current limiting under fault conditions.

Since the reduction ratio required for the eddy current time constant is not large, pole-zero cancellation using a phase-lead compensator[60] is proposed to achieve the necessary reduction. The increase in core resistivity due to elevated temperatures reduces the eddy current time constant and is therefore neglected. The phase-lead compensation should be applied to the electromagnet core flux demand, which incorporates the leakage flux as well as the air gap flux. In a practical system, it would be better to design the electromagnets to have an acceptable eddy current time constant by using either narrower pole pieces, a higher resistivity core material, or laminated cores (see Appendix A). This would reduce the power controller voltage requirement and applies irrespective of the stabilisation strategy used.

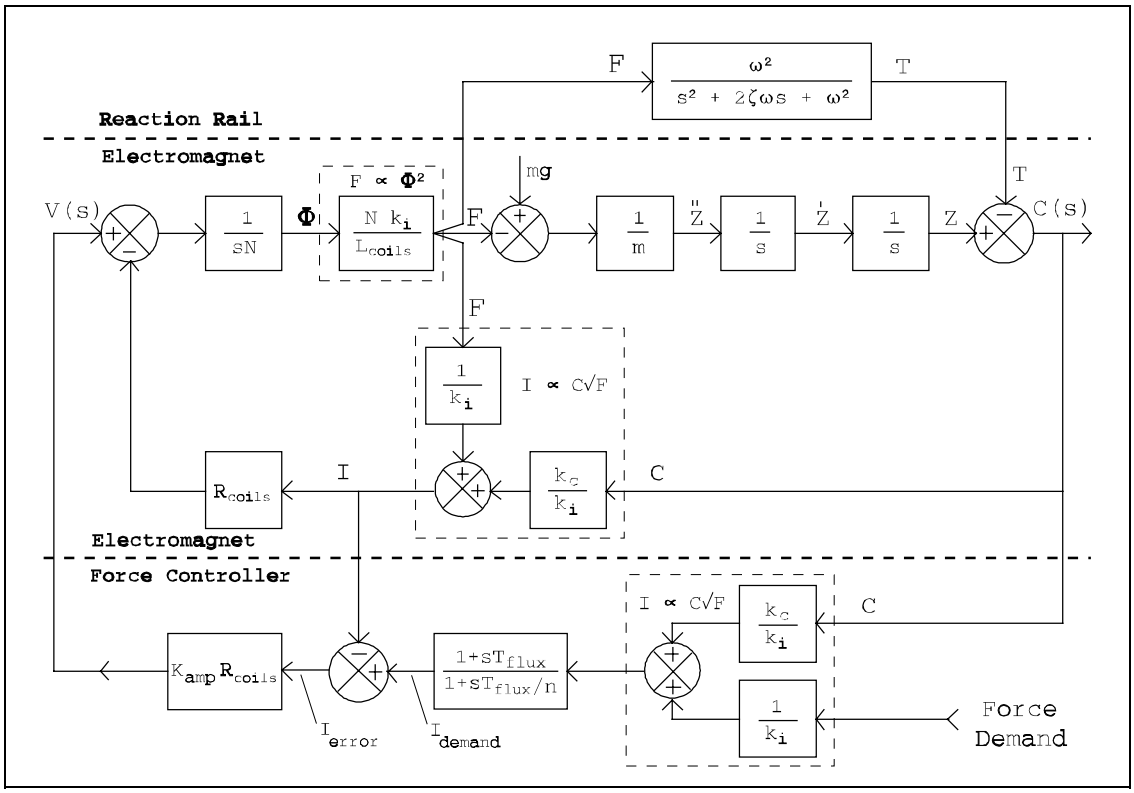

Figure 3.5 Proposed force control configuration

Figure 3.5 illustrates the configuration of the proposed force control strategy. The eddy current flux lag loop has been omitted for the sake of clarity. The detailed design of

the force control algorithm is described next. The implementation of all control system components is described in Chapter 6.

3.5 Force controller design

The stabilisation and linearisation element of the proposed force control strategy consists of feeding the measured air gap and the demanded force into a model of the electromagnet, which then specifies the requisite current demand. The full nonlinear model of the electromagnet is given by Equation 2.20 and is illustrated by Figure 2.7. This equation cannot be used directly because the magnetic reluctance of the electromagnet core depends on the core flux density. Therefore the core flux density must be evaluated en route to the current demand. The full force control algorithm is listed in Figure 3.6, where c is the air gap between the electromagnet and the track, y is the lateral offset between the electromagnet and track poles (which is assumed constant), p is the pole face width, and the air gap, track, leakage and electromagnet reluctances are defined in Chapter 2.

The lateral offset in the control algorithm refers to the fixed pole offset due to the difference in separation between the electromagnet poles and the reaction rail poles. The electromagnet lateral offset is not measured in order to reduce the cost and complexity of the experimental vehicle. Therefore, lateral displacement of the electromagnet relative to the rail, results in a reduction of the suspension lift force. The force reduction does not affect the linearity of the force actuation and only slightly impairs the electromagnet stabilisation function. The same argument applies to the loss of suspension force due to reaction rail eddy currents induced by the electromagnet motion along its guideway.

To increase the open-loop force bandwidth to that required by the suspension controller, the proposed force control strategy employs current feedback and phase-lead compensation of the electromagnet core flux. The required force actuation time constant is about 3.2 ms, whilst the worst-case open-loop coil and eddy current time constants (see Table 3.2) are 111 ms and 4.6 ms respectively. To meet this requirement, a current controller feedback gain of 100 is appropriate to reduce the maximum coil current time constant to a maximum value of about 1.1 ms, giving a total flux lag time constant of 5.7 ms. The total flux lag time constant can be further reduced to a maximum value of 2.5 ms by employing pole-zero cancellation. This is implemented in the controller by applying phase-lead compensation to the electromagnet

$$F_{per\_pole} = \frac{F_{demand}}{2\left(1 - \dfrac{y/c \ \tan^{-1}(y/c)}{1 + \pi p/2c}\right)} \qquad \textit{gross force per pole}$$

$$\Phi_{airgap} = \sqrt{F_{per\_pole} \ \frac{2c}{R_{airgap}(c)}} \qquad \textit{air gap flux}$$

$$M_{airgaps+track} = \Phi_{airgap}\left[2R_{airgap}(c) + R_{track}\right] \qquad \textit{air gap mmfs + track mmf}$$

$$\Phi_{leakage} = M_{airgaps+track} / R_{leakage} \qquad \textit{leakage flux}$$

$$\Phi_{magnet} = \Phi_{airgap} + \Phi_{leakage} \qquad \textit{magnet core flux}$$

$$\Phi_{comp} = Phase\_Lead_{eddy}(\Phi_{magnet}) \qquad \textit{eddy current compensation}$$

$$M_{magnet} = \Phi_{comp} \ R_{magnet}(\Phi_{magnet}) \qquad \textit{magnet core mmf}$$

$$I_{coils} = \left[M_{airgaps+track} + M_{magnet}\right] / N_{coil\_turns} \qquad \textit{current demand}$$

Figure 3.6 Electromagnet force control algorithm (sequential program)

core flux demand using the compensator whose transfer function is given by:

$$Phase\_Lead_{eddy}(s) = \frac{1 + s\,T_{flux}}{1 + s\,T_{flux}/n} \qquad \textit{where } T_{flux} = 5.7\ ms, \ \textit{and } n = 2.3 \qquad \textbf{3.9}$$

The maximum value for the compensated flux time constant of 2.5 ms gives a minimum predicted force actuation bandwidth of about 64 Hz. The actual values used in the experimental system are T_{flux} = 4.6 ms and n = 3, thus giving a slightly higher minimum force bandwidth.

3.6 Force controller performance

The performance of the electromagnet force control algorithm cannot be conveniently tested in isolation due to the residual closed-loop stiffness that always exists due to imperfections in the control algorithm and its implementation. Therefore, a closed-loop air gap controller was used to assist in testing the accuracy, linearity, and stability of a practical implementation of the force control algorithm. The suspension control

system test results presented in Chapter 4 are used to validate the force actuation bandwidth of the experimental force controller.

To impose a realistic test environment on the force controller, the suspension controller developed in Chapter 4 is used to obtain test results for the experimental force controller. The physical arrangement of the experimental single electromagnet suspension rig used for the performance tests is illustrated in Figure 3.7. All measured signals are provided by the control system from the sampled input data.

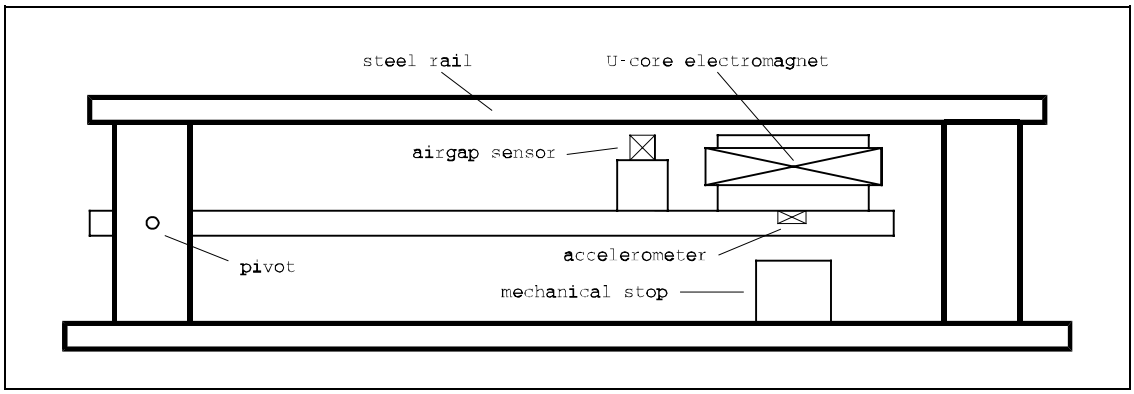

Figure 3.7 Single electromagnet suspension experimental rig

Two tests are used to determine the effectiveness of the force control strategy and implementation. Both tests are performed over the operational range of air gaps and suspension forces. The first test measures the static force accuracy and linearity by plotting measured suspension forces versus reference force demands. The second test determines the residual force actuation stiffness, and hence the residual force instability.

Figure 3.8 illustrates experimental static force measurements for suspended loads of 140, 220, 360 and 510 N. The graph plots the suspension load forces versus the reference force demands required to generate those suspension forces. The measurements were taken over the operational air gap range of 1-5 mm. All of the force measurements are within the anticipated force error tolerance of ±15% except for the 1 mm and 5 mm points with the 510 N load. These are out by just under 19%. The larger error at the 1 mm air gap is attributed to slight bending of the electromagnet support beam which causes air gap measurement errors. The higher error for the maximum air gap is due to the larger inaccuracies involved in modelling the core permeability at the very high core flux level at that operating point.

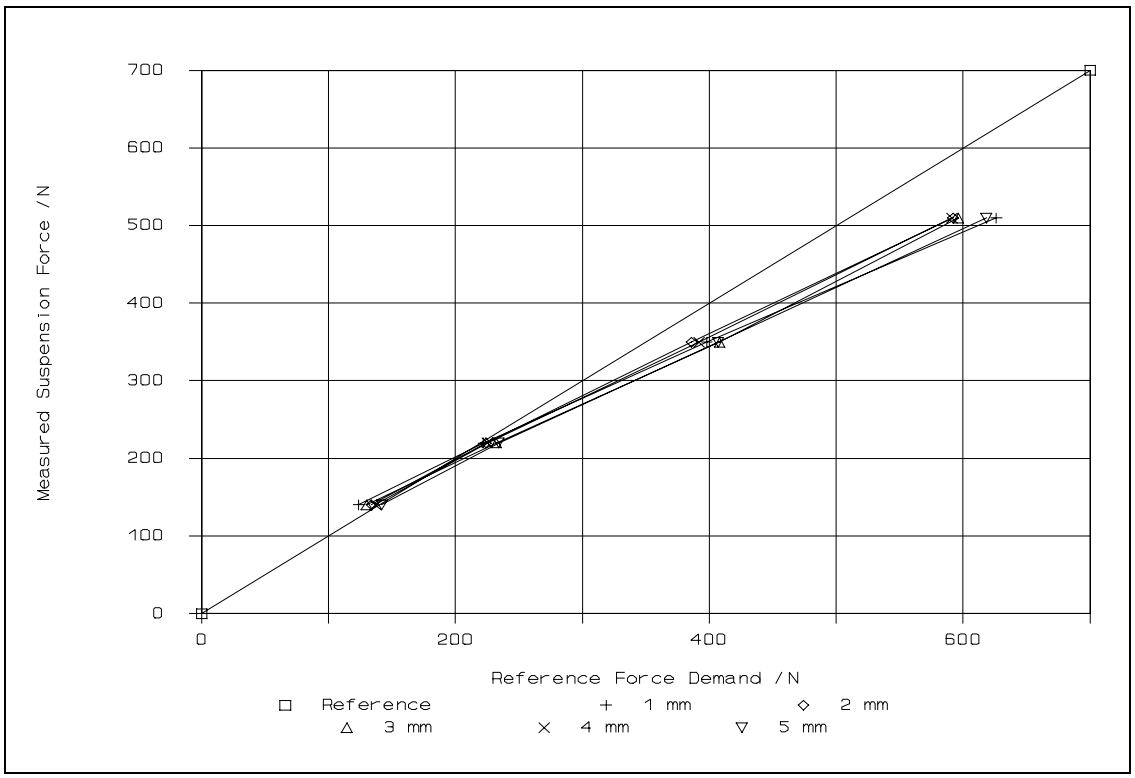

Figure 3.8 Experimental controller reference force demands and actual suspension forces

Figure 3.8 clearly shows that the proposed force controller is successful in producing a dominantly linear static force actuation over the full operational envelope. The force nonlinearity, determined by measuring the maximum deviation from a straight line fitted through all of the experimental data, is typically about ±5%, with a worst case value of ±7% at an air gap of 1 mm.

The residual stiffness exhibited by the force controller is investigated by experimenting with the closed-loop stiffness of the suspension controller by means of the air gap feedback gain. The error integral action is first removed and then the controller air gap feedback gain is reduced to determine the minimum value for which the system remains stable. The worst case electromagnet negative stiffness predicted by Table 3.2 is 950 N/mm, which occurs at maximum load and minimum air gap. For the experimental system, the minimum stable air gap feedback gain for the operating point (1 mm, 510 N) was about 50 N/mm. This represents a residual stiffness of 5% of the predicted electromagnet stiffness. For smaller loads and larger air gaps, the minimum stable air gap feedback gain was approximately 25 N/mm. This result shows that the proposed force control strategy achieves a residual stiffness of 10-20% of the suspension controller stiffness gain of 250 N/mm (see Section 4.4.2).

Table 3.3 summarises the measured performance of the experimental electromagnet force controller in terms of its general accuracy, linearity and residual stiffness. As expected, the performance of the experimental system was found to be highly dependent on the accuracy of the air gap measurement. However, calibration of the air gap sensor offset at the most critical operating point (at a gap of 1 mm), ensured a satisfactory performance from an inexpensive industrial air gap sensor. The impact of magnetic hysteresis is just noticeable at the minimum operational air gap, but it did not significantly impair the behaviour of the force controller.

Table 3.3 Performance of the electromagnet force controller

Parameter	Typical	Worst case
Accuracy	± 15 %	- 19 %
Linearity	± 5 %	± 7 %
Residual stiffness	≤ 25 N/mm	≤ 50 N/mm

3.7 Conclusions

The force/voltage transfer function of the experimental suspension electromagnet has been analysed. Force control schemes employing linear feedback techniques have been shown to be unsuitable for providing independent linear force actuation in an environment where a number of electromagnets are rigidly coupled. Therefore, a new force control algorithm has been proposed, which employs a detailed nonlinear electromagnet model, in conjunction with air gap feedback, to provide an independent force actuator for rigidly coupled electromagnets. The bandwidth of the electromagnet force is increased through the use of closed-loop current feedback and series compensation of the electromagnet core flux.

The proposed electromagnet force control scheme has been shown to possess significant advantages compared with existing stabilisation techniques using flux derivative feedback due to its dominantly linear force actuation. It does however, suffer from a slight disadvantage due to its increased reliance on an accurate air gap measurement at small air gaps. This drawback could be overcome if desired, by developing a hybrid

control approach combining flux derivative feedback, for stability, with the proposed scheme, for force linearity. However, the test results from the experimental implementation of the proposed force control strategy show that an acceptable performance has been achieved. Therefore, this force control strategy will now be used by the suspension control systems described in Chapters 4 and 5.